Transactions on Energy Systems and Engineering Applications

Article

Analysis of rotor bar number on induction motor performance characteristics and rotor temperature

Yasser Mahmoudian[1], Hamid Reza Izadfar[1,*] and Asghar Akbari Foroud[1]

[1] Faculty of Electrical and Computer Engineering, Semnan University, Semnan, Iran
[*] Correspondence: hrizadfar@semnan.ac.ir

Received: 09 September 2024; Accepted: 02 February 2026; Published: 19 March 2026

Abstract: This paper investigates the influence of rotor bar number on the thermal and electromagnetic performance of induction motors using a combined FEM–thermal modeling framework. A systematic analysis covering 8–26 rotor bars was conducted under both constant voltage and constant current conditions. Results show that rotor temperature and torque ripple are strongly dependent on bar count. A multi-objective optimization function is proposed to determine the optimal bar number by balancing efficiency and temperature rise. The novelty of this work lies in integrating thermal constraints into rotor bar selection, providing practical guidance for designers. Validation was performed using Motor-CAD and an extended lumped parameter model, demonstrating good agreement.

© 2026 by the authors. Published by Universidad Tecnológica de Bolívar under the terms of the Creative Commons Attribution 4.0 License. Further distribution of this work must maintain attribution to the author(s) and the published article's title, journal citation, and DOI. https://doi.org/10.32397/tesea.vol7.n1.759

1. Introduction

Due to the robust structure and well-established theory of operation, Induction Motors (IMs) are widely used in the industry [1, 2]. The performance and lifespan of AC IMs have a strong relationship with the motor temperature, and the majority of motor failures caused due to overheating [3]. Accordingly, Thermal analysis has a vital role in motor design, considering its impact on weight, cost, and efficiency. Therefore its significant role in electric motor design is further affirmed [4]. IMs output characteristic prediction can lead to optimizing the motor design to improve its performance [5]. The proper combinations of the rotor bars and stator slots has a strong effect on the characteristics of IMs [6]. Gundogdu et al. [7] conducted a comprehensive study of the influence of the number of rotor bars (NRB) on the waveform of rotor bar current and density, as well as other performance aspects including rotor cage copper loss, efficiency, torque ripple, average torque, etc, has been carried out. Some empirical rules and recommendations have been proposed [8–10] to determine the appropriate slot combinations in terms of parasitic effects such as unbalanced magnetic pull, torque ripple, vibration, acoustic and electromagnetic noise, etc. Gyftakis and Kappatou [11] investigated the effect of different numbers of rotor bars ranging from 24 to 48 on the air-gap flux density, power, torque, efficiency, and power factor.

How to cite this article: Mahmoudian, Yasser; Izadfar, Hamid Reza; Foroud, Asghar Akbari. Analysis of rotor bar number on induction motor performance characteristics and rotor temperature. *Transactions on Energy Systems and Engineering Applications*, 7(1): 759, 2026. DOI:10.32397/tesea.vol7.n1.759

In this paper, the effect of rotor bar number on rotor temperature is evaluated. An extended lumped parameter thermal model (LPTM) of IM [12] is used to examine machine temperatures. The machine can be divided into several components to generate a thermal model. The heat transfer coefficients of convection and conduction, as well as heat storage capacity, can be evaluated for each type of system [13–17]. To accurately determine the machine's thermal parameters, the material's dimensions and characteristics must be specified [18]. There are several heat sources as windings and core iron losses in an IM [19]. With only one heat source and one energy storage, an estimation of temperature can be conducted even with a simple model [20].

This paper studies the effects of the rotor bar number on the rotor temperature and characteristics of a 1.1kW, 2-pole, 3-phase IM using FEM analysis. The stator used for the simulation was chosen from an IM in the laboratory whose geometrical variables were known. Then the results from 20 simulations with different rotor bar numbers varying between 8 to 26 bars have been represented and discussed. From the point of view of IM design, changing the number of bars in this range is certainly not correct. However, our goal of this analysis is to show that the correct proportion of stator and rotor slots affects the thermal quality of the motor and some other parameters such as ripple torque and so on.

Simulations were performed in two different cases. In each case to achieve a comparable result, the same operating conditions and the same motor geometric parameters as well as winding layout, are used in all calculations. In the first case, the applied voltage to the motor is kept constant in all simulations, and in the second case, the simulations were performed assuming the stator current remained constant.

After extracting the output characteristics of the motor, the effect of the NRB on the rotor temperature in different modes is investigated and analyzed utilizing an extended LPTM. Also, to validate the results, the motor with a different NRB is simulated in the Motor-CAD software. Finally, to find the optimal NRB based on the specific operating conditions considered by a designer, an objective function is defined which, has been solved for a specific operating condition of the sample motor, and the results are presented.

In Section 2, the motor specifications, simulation methodology, and the approach for studying the impact of rotor bar variations on motor characteristics are presented. In Section 3, the rotor bars are changed while maintaining a constant applied voltage to the motor in all cases. The motor's performance characteristics are then extracted and analyzed. Additionally, an optimization function is introduced to enable motor designers to determine the optimal number of rotor bars based on the motor's operating conditions. In Section 4, the same procedure is carried out while keeping the motor's input current constant, and in Section 5, the study's findings are presented.

2. Induction Motor Analysis

This section describes the analytical and numerical procedures used to investigate the influence of the rotor bar number (NRB) on the electromagnetic and thermal behavior of the induction motor (IM). The methodology combines finite element analysis (FEM), a modified lumped parameter thermal model (LPTM), and validation using Motor-CAD software.

2.1. Motor Specifications

The investigated motor is a three-phase, 1.1 kW, two-pole squirrel-cage induction motor with 18 stator slots and 16 rotor bars in its reference design. The geometrical parameters of the stator and rotor were extracted from an experimental prototype available in the laboratory. Table 1 presents the key specifications of the tested motor.

To analyze the impact of NRB variation, rotor bar numbers were systematically changed from 8 to 26 in steps of 2. Although this range exceeds typical industrial values (generally 14–24 bars), it was intentionally

selected to provide a broader theoretical understanding of bar number effects on both electromagnetic and thermal characteristics.

Table 1. Squirrel cage IM parameters

Parameter	Value
Power	1.1 kW
Voltage	380 V
Frequency	50 Hz
Nominal Current	2.48 A
Pole number	2
Number of stator slot	18

2.2. Electromagnetic Modeling

The electromagnetic field of the IM was modeled in Ansys Maxwell 2D using the finite element method. The model incorporated accurate geometric dimensions, slot shapes, and material properties for both stator and rotor components. The air gap, copper, and core losses were computed under sinusoidal supply conditions. Figure 1 illustrates the main motor simulation. The electromagnetic analysis provides key outputs such as flux density distribution, stator and rotor current waveforms, electromagnetic torque and copper and core losses.

These outputs form the input heat sources for the thermal model described in the next subsection. The analysis was performed under two operating scenarios:

1. Constant voltage: the input voltage remains fixed for all NRB values.
2. Constant current: the stator current amplitude is kept constant across all simulations.

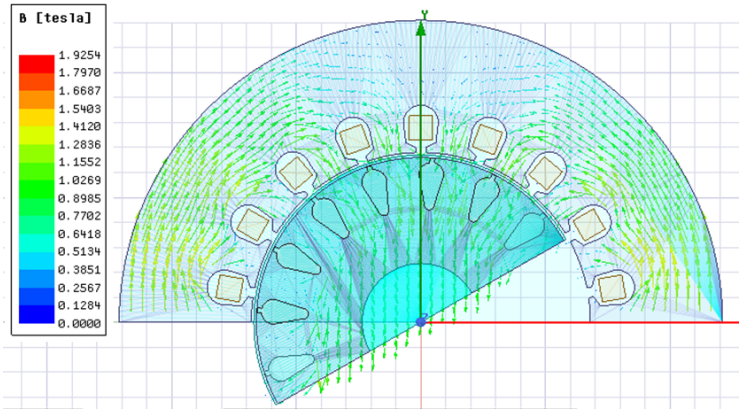

Figure 1. IM model in Maxwell software

2.3. Thermal Modeling

To estimate the temperature distribution in the machine, an extended Lumped Parameter Thermal Model (LPTM) was developed based on the equivalent thermal resistances and capacitances of the main components—stator core, stator winding, rotor cage, shaft, and air gap.

The thermal resistances were calculated from the material properties, geometry, and heat transfer coefficients. The heat sources obtained from the FEM analysis (rotor and stator losses) were applied to the model to predict the temperature rise in each component.

The main advantages of the LPTM approach are:

- Low computational cost compared to full 3D CFD models
- Ability to couple directly with electromagnetic loss data
- Flexibility for design optimization

Temperature results obtained from the thermal model were cross-verified with Motor-CAD simulations to ensure accuracy. Figure 2 shows the experimental test bench used for validating the temperature measurements.

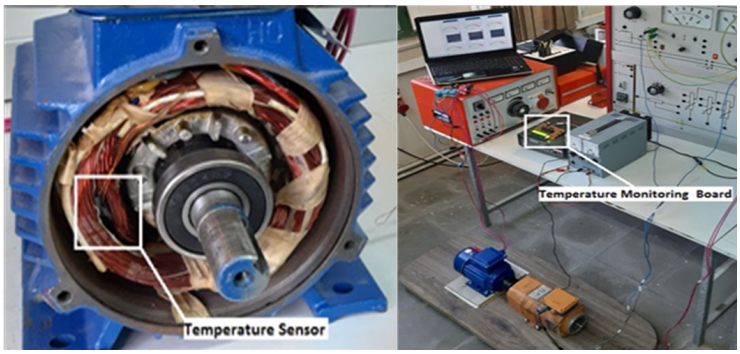

Figure 2. Test bench of IM and temperature metering hardware

2.4. Coupled Electromagnetic–Thermal Workflow

The overall simulation process is illustrated in Figure 3, which shows the interaction between the FEM analysis, thermal model, and optimization algorithm.

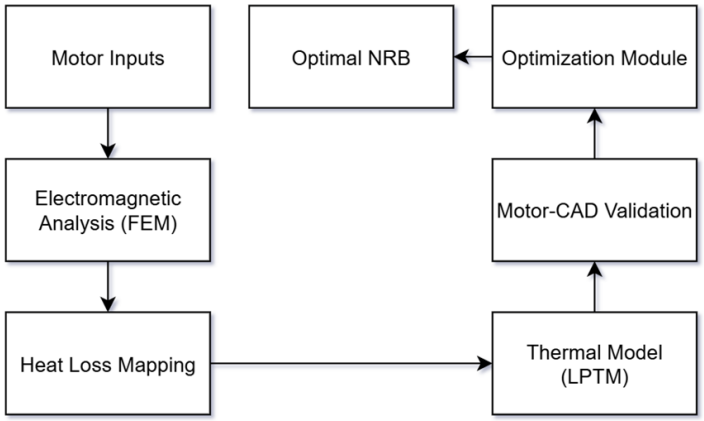

Figure 3. Workflow of the electromagnetic–thermal analysis and optimization process

2.5. Validation Procedure

To verify the reliability of the coupled analysis, the following validation steps were performed:

Experimental temperature measurements were taken from the stator winding using thermocouples during rated operation. The LPTM and Motor-CAD temperature results were compared with these measurements, showing less than 3% deviation in steady-state conditions.

This validation confirms that the combined FEM–LPTM framework can predict rotor temperature trends with sufficient accuracy for design and optimization purposes. The validated electromagnetic–thermal framework was then used to analyze the effect of rotor bar number on motor performance under both constant voltage and constant current conditions, as presented in Section 3.

3. Analysis Under Constant Input Voltage

In this section, the rotor bars are changed while maintaining a constant applied voltage to the motor in all scenarios. Subsequently, the motor's performance characteristics were evaluated, and the resulting variations were analyzed. Finally, the rotor temperature is obtained by using the extended LPTM and the Motor-CAD software to validate the results. The effect of the number of motor bars on the torque amplitude, torque ripple, losses, efficiency, power factor, losses, and heat generated in the rotor, will be introduced.

3.1. Effect of NRB on motor performance characteristics

Assuming constant voltage, the effects of the change of bar numbers have been simulated and analyzed. Simulation has been done for the values of 8 to 26 bars. The magnitude of the stator in these cases is shown in Figure 4. According to it, as the NRB increases, the motor input current increases significantly. By increasing the number of bars, the equivalent resistance equivalent of the rotor and therefor the impedance of the motor decreases and this will increase the current. The change of NRB also affects on harmonic distortion of currents. The variation in harmonic distortion with the number of rotor bars can be theoretically explained by the interaction between stator and rotor slot harmonics. The spatial harmonic order in the air gap is expressed as $h = kN_s \pm p$ where N_s is the stator slot number, p is the pole-pair number, and k is an integer representing the harmonic index. When the ratio between stator slots and rotor bars approaches an integer, some harmonics coincide, causing magnetic coupling and increased current distortion. Conversely, increasing the number of rotor bars shifts the harmonic frequencies to higher orders, thereby reducing low-order harmonics that mainly contribute to torque ripple and total harmonic distortion (THD). However, when $N_r = N_s$, strong coupling occurs, leading to pronounced distortion and acoustic noise. This behavior is consistent with the theoretical analyses reported in [21–23]. According to Figure 5, for 12 and 22 bars, less distortion in the current has occurred. The waveform of stator current for 12, 18, and 22 rotor bars is plotted in Figure 6.

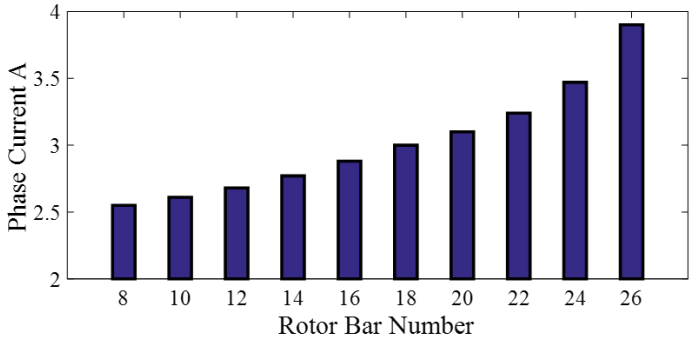

Figure 4. Variation of stator current

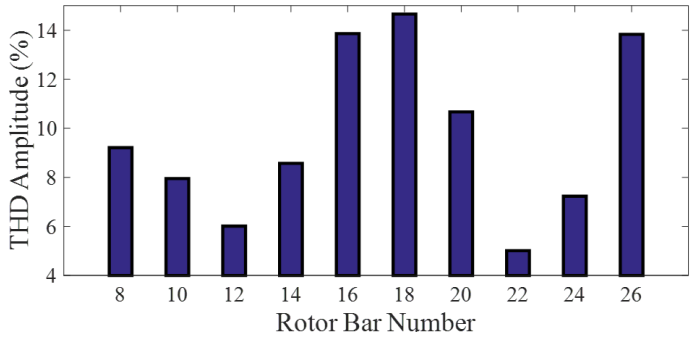

Figure 5. Variation of stator current THD

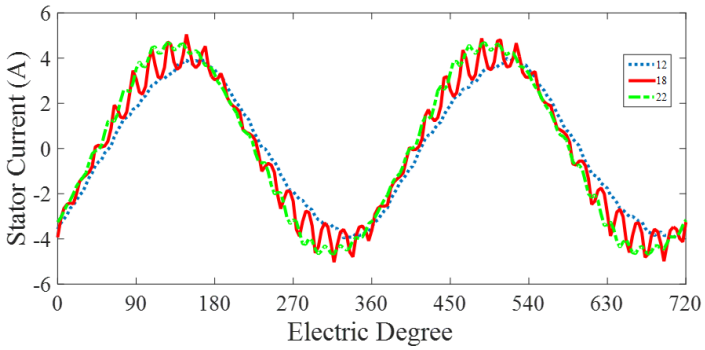

Figure 6. Phase A stator current waveform

The current distortion in the rotor bars is highly dependent on the ratio of the number of bars to the number of poles [24]. Furthermore, recent studies have demonstrated that the rotor bar current can become non-sinusoidal under specific operating conditions, such as low slip, significant loading, or a small air gap length [25, 26]. Another critical characteristic of the induction machine is the electromagnetic torque. Its variation is illustrated in Figure 7. In the design of the IM rotor, determining the NRB and their geometry is one of the most crucial factors, as it directly affects noise, vibration, torque density, and torque ripple. As shown in Figure 7, the electromagnetic torque increases with the number of bars. The variation of torque ripple is presented in Figure 8. The results demonstrate that the torque ripple increases when the NRB equals the number of stator slots. Torque ripple induces vibration and acoustic noise, which directly impacts the machine's failure rate and service life.

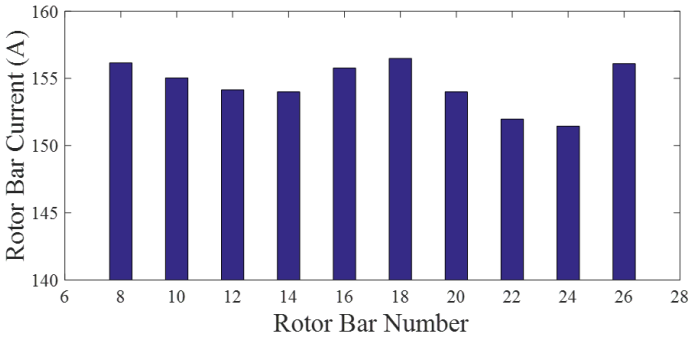

Figure 7. Variation of rotor bar current

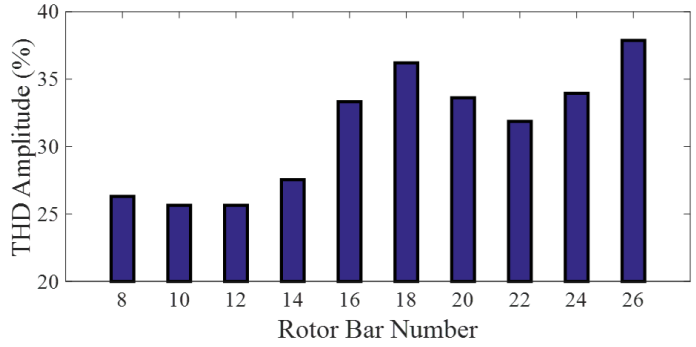

Figure 8. Variation of rotor bar current THD

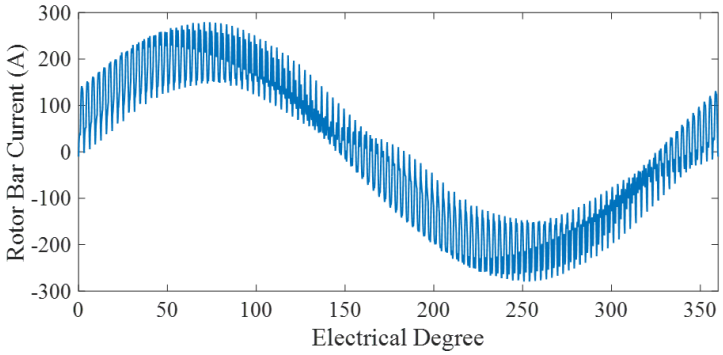

Figure 9. Current of rotor bars in the case of 14 rotor bars

Another performance characteristic of the IM is the torque; which changes are shown in Figure 10, With regards to torque quality and density, some key parameters such as pole and stator slot number combinations considering the long- and short-pitch winding layout, and stator/rotor slot opening should be optimized either.

In designing the IM rotor, determining the NRB and their geometry is one of the most crucial factors that determine noise, vibration, torque density, and torque ripple. As shown in Figure 9, the electromagnetic torque increases with the number of bars. The variation of torque ripple is presented in Figure 11. As demonstrated, the torque ripple increases when the NRB and the stator slot are equal.

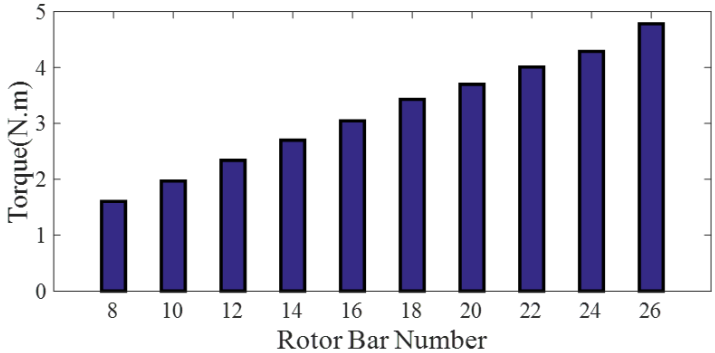

Figure 10. Variation of the average torque

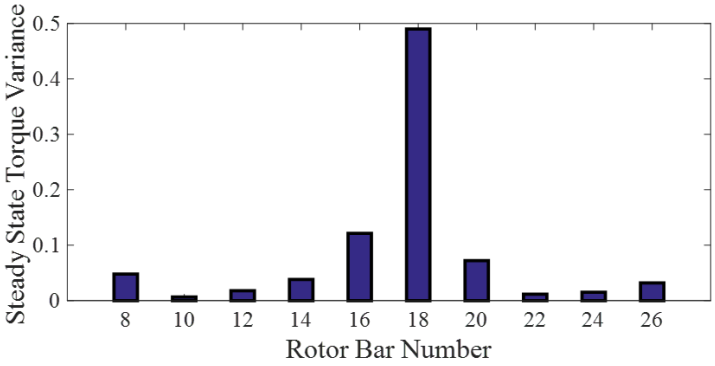

Figure 11. Variation of the torque ripple

Torque ripple will cause vibration and acoustic noise, which will have a direct impact on the failure rate and life of the machine. The electromagnetic torque waveforms in the case of 14, 18, and 22 rotor bars are plotted in Figure 12. As can be seen, there is a large amount of distortion of the motor torque in the case of an equal number of rotor and stator slots.

Figure 13 shows the power factor variation and the efficiency changes are shown in Figure 14. Based on Figures 13 and 14, 22 rotor bars provide a better power factor and higher efficiency. Figure 15 illustrates the variation of stator winding losses, core losses, and rotor cage losses.

Core losses remained constant as long as the voltage was constant, but due to the increase in the motor input current amplitude, the stator winding losses have increased significantly. In addition, despite the small changes in the current of the rotor bars, increasing the number of bars has led to an increase in rotor cage losses. Therefore, by raising the NRB, the total motor losses will have increased.

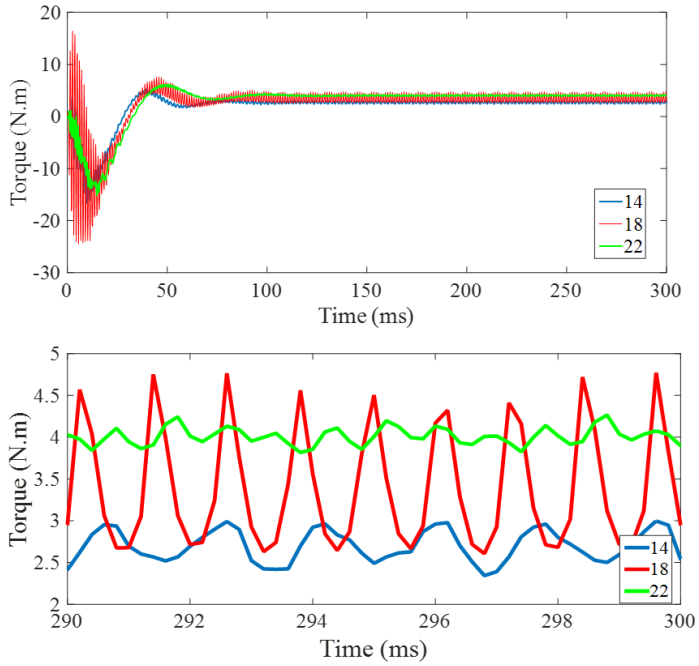

Figure 12. Electromagnetic torque waveforms in the case of 14, 18, and 22 rotor bar

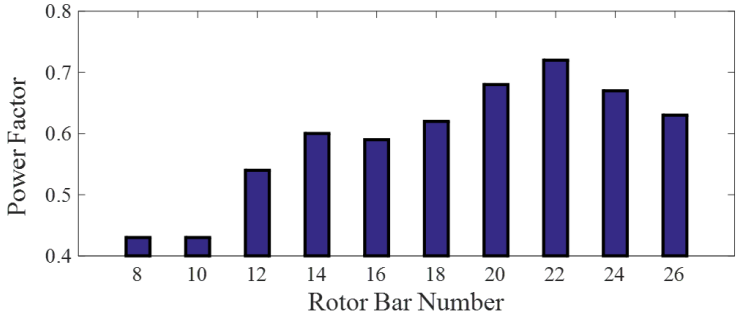

Figure 13. Variation of power factor

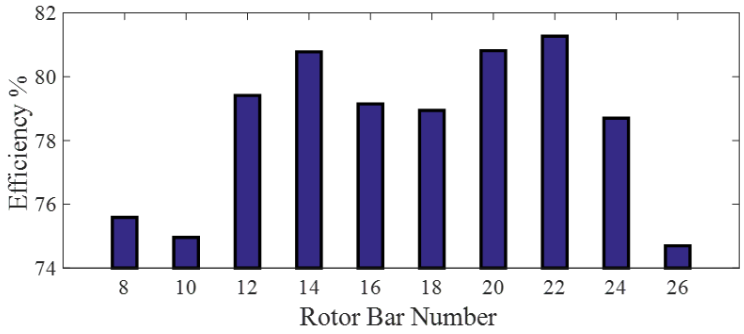

Figure 14. Variation of efficiency

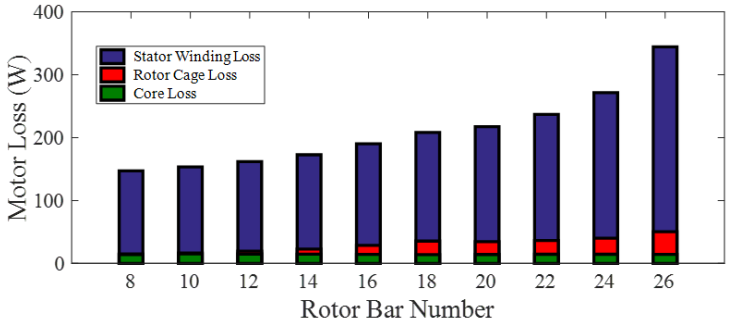

Figure 15. Variation of motor losses

By losses calculated for different numbers of rotor bars, the rotor temperature can be calculated by the LPTM and also Motor-CAD software. Figure 16 Shows the Motor-CAD simulation results in the case of 24 rotor bars. The obtained temperature for the rotor by the thermal model and Motor-CAD software for different numbers of rotor bars are shown in Table 2. The rotor temperature variation is shown in Figure 17. As can be seen, the rotor temperature increases significantly upon the number of the bar.

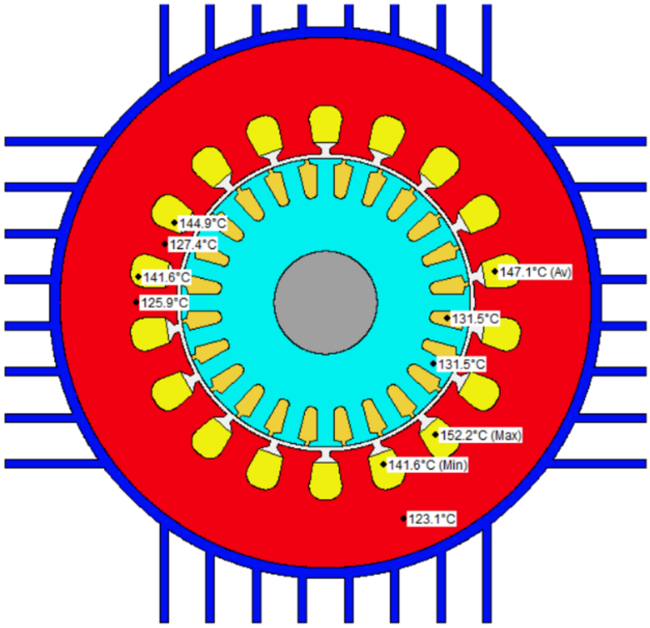

Figure 16. Motor-CAD simulation results in the case of 24 rotor bars

Table 2. Variation of rotor temperature

Rotor bars Number	Thermal Model Rotor Temp (°C)	Motor-CAD Rotor Temp (°C)
8	76.9	75
10	80.12	81
12	85.99	85.9
14	92.86	91.5
16	104.56	101
18	113.1	111.4
20	117.55	113.1
22	122.37	119.6
24	132.32	131.5
26	157.39	157.5

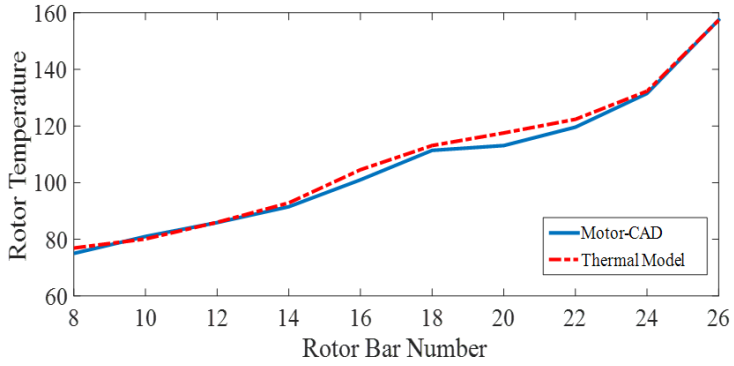

Figure 17. Variation of rotor temperature

3.2. Finding optimal NRB

According to the parameters such as efficiency, average torque, torque ripple, power factor, motor temperature, etc., the number of optimal bars for examining IM can be determined by defining the objective function according to Equation 1.

$$Min\ F(n) = w_1\left(\frac{T}{T_{desired}} - 1\right)^2 + w_2\left(\frac{\eta}{\eta_{desired}} - 1\right)^2 + w_3\left(\frac{\tau}{\tau_{desired}} - 1\right)^2 + \dots \tag{1}$$

Where T is the rotor temperature (in °C), η efficiency, τ torque (in N.m), and w_1 to w_3 are the weights that determine the importance of each characteristic in the design process.

Weight is defined for each of the motor performance characteristics, which the designer determines depending on the operating conditions of the motor and the importance of improving each of the motor features.

To find the optimal state for efficiency and temperature, the above equation is revised and solved as Equation 2 for $\eta_{desired} = 79\%$ and $T_{desired} = 90°C$. Figure 18 shows the fitness values versus bar numbers and weight w. As demonstrated, for each desired weight depending on the motor design conditions, there is a minimum point that provides the optimal number of motor bars to satisfy the designer's desired conditions.

$$Min\ F(n) = w\left(\frac{T}{90} - 1\right)^2 + (1-w)\left(\frac{\eta}{79} - 1\right)^2 \tag{2}$$

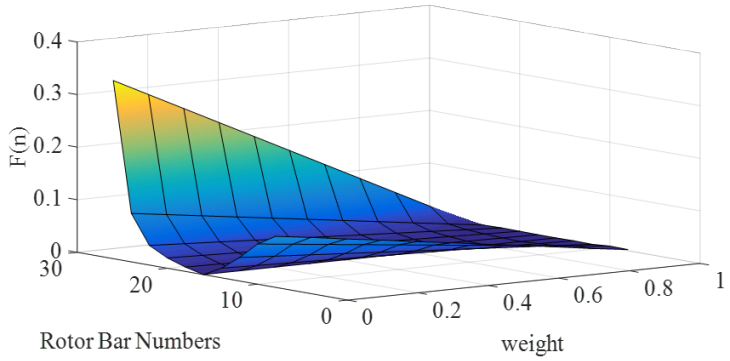

Figure 18. Solving optimization function for rotor bar number and desired weight

4. Analysis Under Constant Input Current

In this section, the rotor bars are altered while ensuring that the input current to the motor remains constant in all cases. The motor's performance characteristics are then extracted and analyzed to assess the resulting variations. Finally, the rotor temperature is determined using the extended LPTM and validated through Motor-CAD software. Additionally, the impact of the number of rotor bars on torque amplitude, torque ripple, losses, efficiency, power factor, and heat generation in the rotor is analyzed.

4.1. Effect of NRB on motor performance characteristics

The simulations were carried out under the assumption of a constant input current. Figure 19(a) illustrates the variation of the stator induced voltage with respect to the rotor bar number, while Figure 19(b)

presents the corresponding voltage waveforms for motors with 8, 16, and 26 rotor bars. As can be observed, the magnitude of the stator induced voltage decreases as the number of rotor bars increases. The voltage waveforms exhibit noticeable distortion, which arises from the combined effects of slotting and magnetomotive force harmonics.

The rotor bar current variation and its corresponding THD are depicted in Figures 20 and 21. It can be seen that the rotor bar current amplitude decreases with an increasing number of rotor bars. According to Figure 21, motors with 26 rotor bars experience greater harmonic distortion compared to those with fewer bars. Figure 22 shows the rotor bar current waveforms for 8 and 26 rotor bars, respectively. As can be observed, the current waveforms are distinctly non-sinusoidal, exhibiting harmonic distortion primarily caused by slot harmonics and magnetic coupling effects, as discussed in Section 2.1.

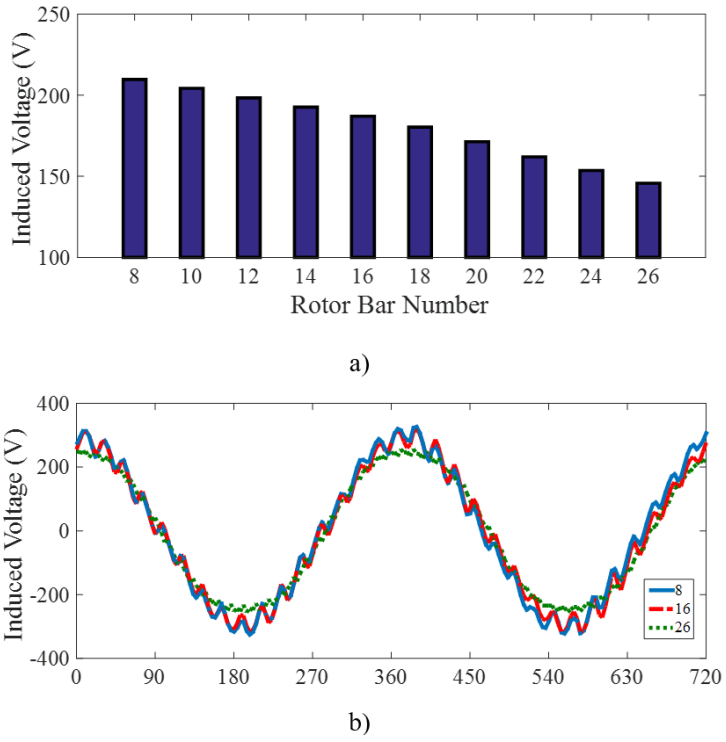

Figure 19. The induced voltage in the stator winding (a) RMS value for rotor bar number (b) voltage waveform

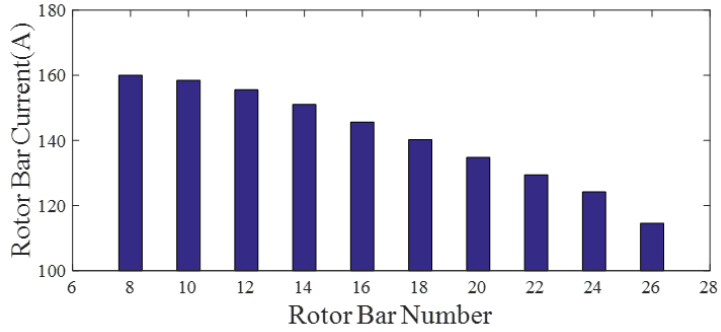

Figure 20. Variation of rotor bar current

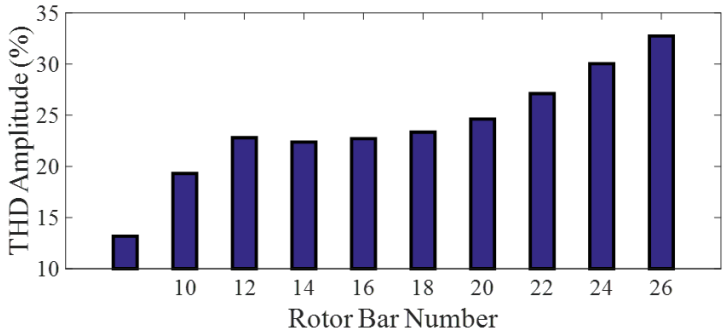

Figure 21. Variation of rotor bar current THD

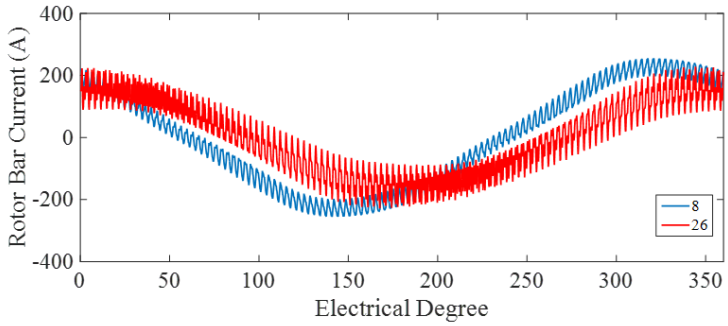

Figure 22. Rotor bar current waveforms for 8 and 26 rotor bars

Variations of average torque concerning rotor bar number are shown in Figure 23. The maximum torque is obtained in the 20 and 22-rotor bars. Figure 24 shows the torque ripple. If the number of rotor and stator slots is equal, we will have the maximum torque ripple. To avoid torque ripple, and noisy operation, the number of rotor and stator slots should not be equal. Figure 25 shows the motor torque for 10 and 18 rotor bars. The high torque ripple in the case of 18 rotor bars is well illustrated in Figure 25 (b).

The variations of power factor and efficiency versus to bars number have been shown in Figures 26 and 27, respectively. According to Figure 26, as the NRB increases, the motor power factor improves. Efficiency is also relatively increasing. The highest efficiency is achieved in the case of 20 rotor bars. Figure 27 illustrates the variation of core losses and rotor cage losses.

The core losses have decreased due to the reduction of the motor input voltage, but despite the decrease in the current of the rotor bars, due to the increase in the number of these bars, the total losses of the rotor cage have increased. Due to the constant stator current, the stator winding losses remain constant in all states. In general, as the NRB increases, the total motor losses will increase.

Using the losses obtained for various numbers of rotor bars, the rotor temperature is calculated by the extended LPTM and also by simulation in Motor-CAD software. Figure 29 Shows the Motor-CAD simulation results in the case of 24 rotor bars. Table 3, shows the Variation of rotor temperature concerning rotor bar number.

As can be seen, assuming the stator current remains constant, the rotor temperature increases significantly as the NRB increases. Therefore, with increasing the NRB, despite increasing the motor torque and improving the torque ripple, the motor temperature increases severely. The rotor temperature variation is shown in Figure 30.

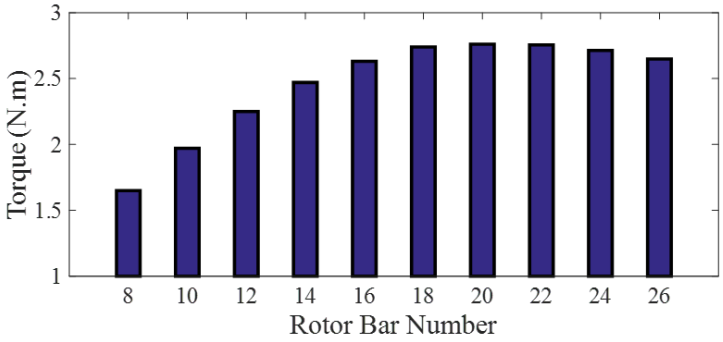

Figure 23. Variation of average torque

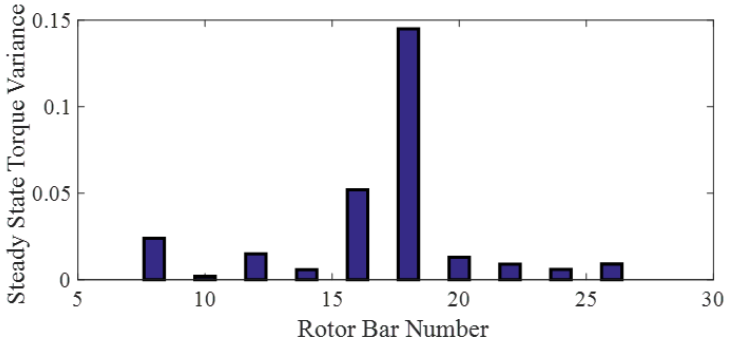

Figure 24. Variation of torque ripple

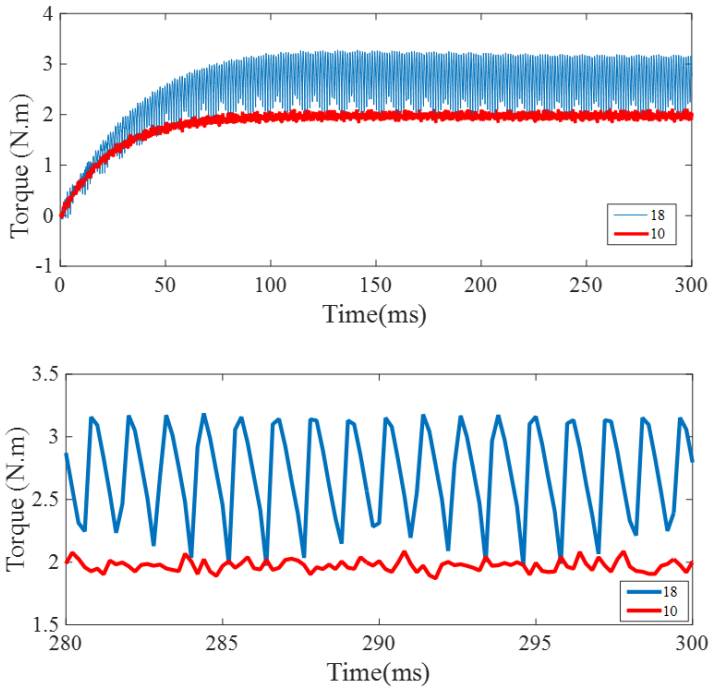

Figure 25. Electromagnetic torque waveforms in the case of 10 and 18-rotor bar

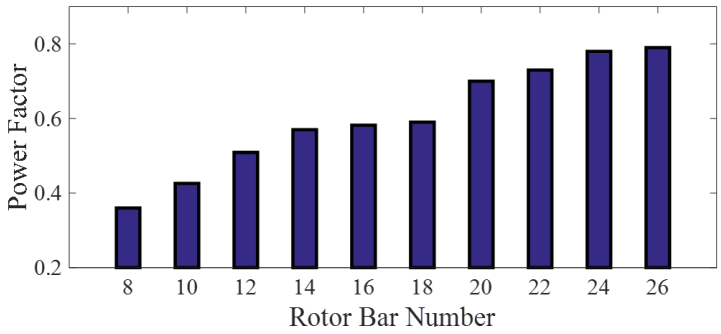

Figure 26. Variation of power factor

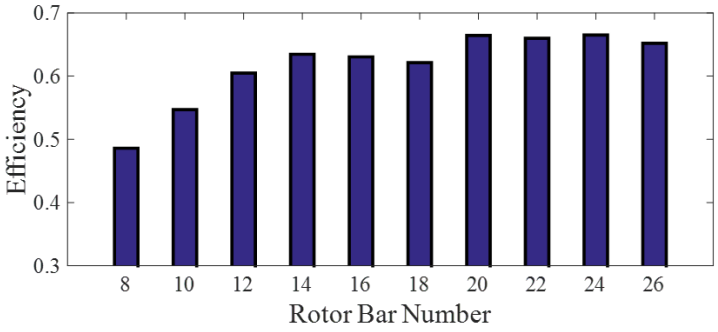

Figure 27. Variation of efficiency

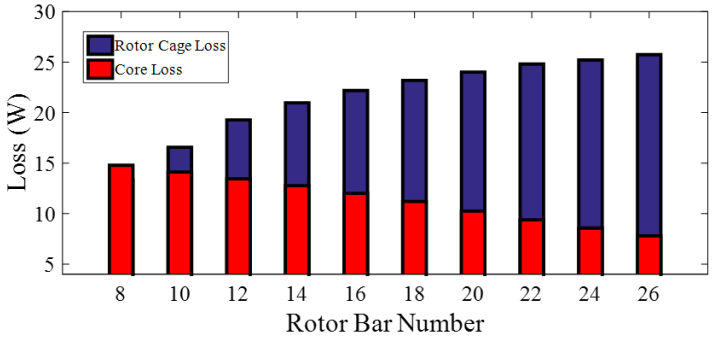

Figure 28. Variation of rotor cage and core losses

4.2. Finding optimal NRB

In this section, according to (1), the optimal NRB can be obtained depending on the different operating conditions of the IM according to the discretion of the machine designer. To get a better view of the results of solving (1), for the case $\eta_{desired} = 65\%$ and $T_{desired} = 82^{\circ C}$ (1) rewrite as (3) and solve.

Figure 31 is drawn in a three-dimensional device for different weights w. As shown, for each desired weight, depending on the motor design conditions, there is a minimum point that provides the optimal number of motor bars to satisfy the designer's desired conditions.

$$Min\ F(n) = w(T/82 - 1)^2 + (1 - w)(\eta/65 - 1)^2 \tag{3}$$

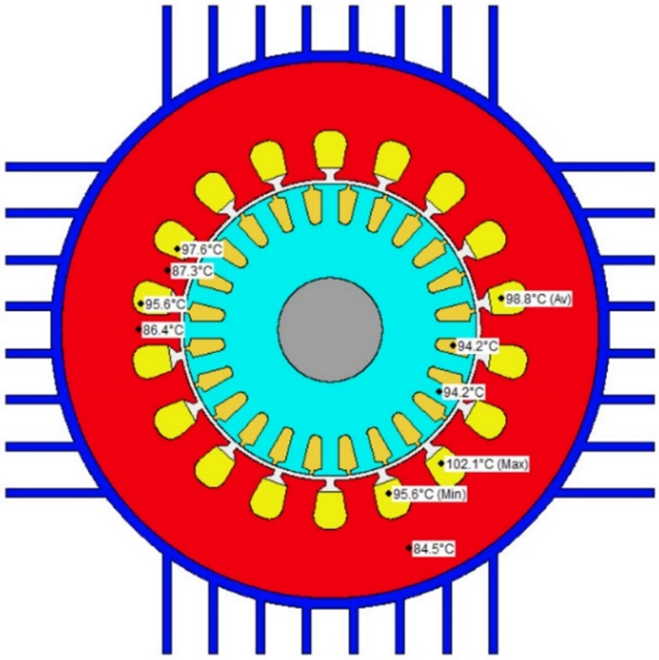

Figure 29. Motor-CAD simulation results in the case of 24 rotor bars

Table 3. Rotor temperature under constant current

Rotor bars Number	Thermal Model Rotor Temp (°C)	Motor-CAD Rotor Temp (°C)
8	72.5	71.8
10	75.3	74.9
12	79.1	78.5
14	83.6	82.9
16	89.2	88.7
18	95.8	95.1
20	99.4	98.6
22	103.7	103.0
24	110.2	109.5
26	120.8	120.1

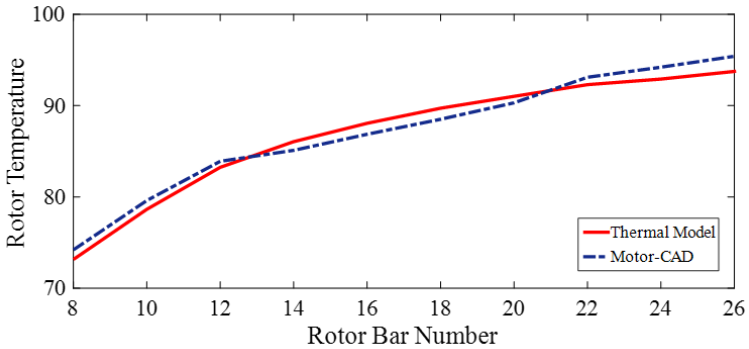

Figure 30. Variation of rotor temperature

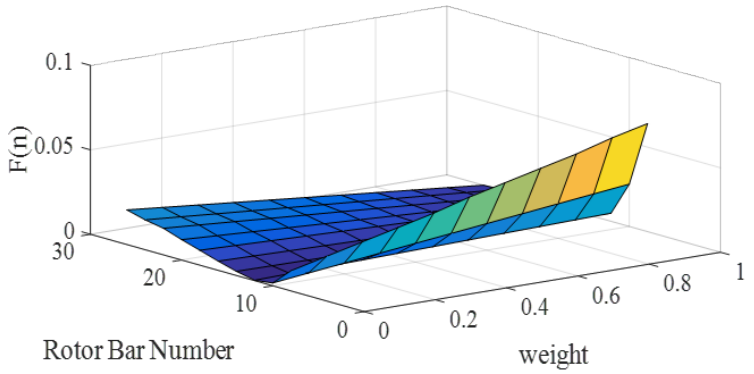

Figure 31. Solving Optimization function concerning rotor bar number and desired weight

5. Practical Applicability and Limitations

The overall findings of this study reveal a clear trade-off between torque enhancement and thermal performance. Increasing the rotor bar number improves torque and efficiency but causes higher copper losses and rotor temperature. Recent studies further reinforce these conclusions. Goman et al. [27] demonstrated that electromagnetic–thermal coupling is essential to predict realistic temperature distributions, while Mahmouditabar and Baker [28] reported that optimizing rotor slot and bar geometry significantly improves heat dissipation efficiency. Similarly, Zhao et al. [29] and Gronwald and Kern [30] showed that neglecting transient thermal effects could underestimate rotor temperature by up to 6%.

When more emphasis is placed on efficiency (lower weighting for temperature), the optimal number of bars shifts toward higher values (22–24). Conversely, prioritizing thermal safety yields an optimal value of approximately 20 bars.

The proposed optimization framework thus provides a flexible and practical approach for balancing design priorities in induction motor development.

The developed electromagnetic–thermal coupled model and optimization framework can be directly applied to small and medium-size industrial induction motors used in pumps, compressors, and fans. It enables designers to consider both electromagnetic and thermal constraints early in the design stage, reducing prototype iterations and design time.

However, the current work is subject to several limitations:

1. **Steady-state assumption:** The model neglects transient heat transfer effects.
2. **Single machine validation:** The model was validated using one motor prototype. Extending it to motors with different ratings or frame sizes will enhance generalization.
3. **Manufacturing constraints:** Mechanical tolerances, rotor slot fill factors, and cost factors were not included in the optimization. These aspects will be integrated in future research.

Despite these limitations, the methodology offers a robust foundation for multi-physics-based design optimization of induction motors, providing a clear pathway for future enhancement.

6. Conclusions

This study investigated the influence of rotor bar number on the electromagnetic and thermal performance of induction motors. Using finite element analysis and an extended lumped parameter thermal model, it was shown that increasing the rotor bar number enhances torque and efficiency but simultaneously raises rotor temperature. An optimization function was developed to identify the best

trade-off between performance and thermal constraints. The results demonstrated that for the studied 1.1 kW motor, 20–22 rotor bars provide a favorable balance between efficiency, torque ripple, and temperature rise. Practically, the proposed approach helps designers consider both electromagnetic and thermal effects when selecting rotor configurations. The study is limited to steady-state analysis and a single motor prototype; future work will extend the model to transient thermal behavior and other motor ratings.

Funding: This research received no external funding.

Author contributions: [Mahmoudian]: Conceptualization, Methodology, Software, Investigation, Writing - Original Draft. [Izadfar]: Conceptualization, validation, Project administration, Writing-Reviewing and Editing, Supervision. [Akbari Foroud]: Supervision, Validation. All authors read and approved the final manuscript.

Disclosure statement: The authors have no competing interests to declare relevant to this article's content.

References

[1] Amin Hasanzadeh, David M. Reed, and Heath F. Hofmann. Rotor resistance estimation for induction machines using carrier signal injection with minimized torque ripple. *IEEE Transactions on Energy Conversion*, 34(2):942–951, June 2019.

[2] Hassan H. Eldeeb, Alberto Berzoy, and Osama Mohammed. Stator fault detection on dtc-driven im via magnetic signatures aided by 2-d fea co-simulation. *IEEE Transactions on Magnetics*, 55(6):1–5, June 2019.

[3] Haisen Zhao, Hassan H. Eldeeb, Jinyu Wang, Jinping Kang, Yang Zhan, Guorui Xu, and Osama A. Mohammed. Parameter identification based online noninvasive estimation of rotor temperature in induction motors. *IEEE Transactions on Industry Applications*, 57(1):417–426, January 2021.

[4] D. Staton, M. Popescu, C. Cossar, M. McGilp, S. Omori, and T. Kurimoto. Analytical thermal models for small induction motors. In *2008 18th International Conference on Electrical Machines*, page 1–6. IEEE, September 2008.

[5] Chengliu Ai, Xian Cao, and Haifeng Wang. Analysis of a 1.5kw induction motor through electromagnetic and thermal simulations. In *2021 3rd Asia Energy and Electrical Engineering Symposium (AEEES)*, page 249–254. IEEE, March 2021.

[6] Gojko Joksimovic, Emil Levi, Aldin Kajevic, Mario Mezzarobba, and Alberto Tessarolo. Optimal selection of rotor bar number for minimizing torque and current pulsations due to rotor slot harmonics in three-phase cage induction motors. *IEEE Access*, 8:228572–228585, 2020.

[7] T. Gundogdu, Z. Q. Zhu, and J. C. Mipo. Influence of rotor slot number on rotor bar current waveform and performance in induction machines. In *2017 20th International Conference on Electrical Machines and Systems (ICEMS)*. IEEE, August 2017.

[8] Byung-Taek Kim, Byun-Il Kwon, and Seung-Chan Park. Reduction of electromagnetic force harmonics in asynchronous traction motor by adapting the rotor slot number. *IEEE Transactions on Magnetics*, 35(5):3742–3744, 1999.

[9] K.S. Huang, Z.G. Liu, H. Li, J. Yang, D.R. Turner, L. Jiang, and Q.H. Wu. Reduction of electromagnetic noise in three-phase induction motors. In *Proceedings. International Conference on Power System Technology*, volume 2 of *ICPST-02*, page 745–749. IEEE.

[10] T. Kobayashi, F. Tajima, M. Ito, and S. Shibukawa. Effects of slot combination on acoustic noise from induction motors. *IEEE Transactions on Magnetics*, 33(2):2101–2104, March 1997.

[11] Konstantinos N. Gyftakis and Joya Kappatou. The impact of the rotor slot number on the behaviour of the induction motor. *Advances in Power Electronics*, 2013:1–9, February 2013.

[12] Yasser Mahmoudian, Hamid Reza Izadfar, and Asghar Akbari Foroud. Introduction of a modified thermal model for squirrel cage induction motor based on calculation of rotor bars' current. *Electrical Engineering*, 105(1):141–150, October 2022.

[13] C. Kral, T.G. Habetler, R.G. Harley, F. Pirker, G. Pascoli, H. Oberguggenberger, and C.-J.M. Fenz. Rotor temperature estimation of squirrel-cage induction motors by means of a combined scheme of parameter estimation and a thermal equivalent model. *IEEE Transactions on Industry Applications*, 40(4):1049–1057, July 2004.

[14] Yi Huang and Clemens Gühmann. Temperature estimation of induction machines based on wireless sensor networks. *Journal of Sensors and Sensor Systems*, 7(1):267–280, April 2018.

[15] Z. Lazarevic, R. Radosavljevic, and P. Osmokrovic. A novel approach for temperature estimation in squirrel-cage induction motor without sensors. *IEEE Transactions on Instrumentation and Measurement*, 48(3):753–757, June 1999.

[16] Zhi Gao, T.G. Habetler, and R.G. Harley. A complex space vector approach to rotor temperature estimation for line-connected induction machines with impaired cooling. *IEEE Transactions on Industrial Electronics*, 56(1):239–247, January 2009.

[17] Anton Haumer, Christian Kral, Vladimir Vukovic, Alexander David, Christian Hettfleisch, and Attila Huzsvar. A parametrization scheme for high performance thermal models of electric machines using modelica. *IFAC Proceedings Volumes*, 45(2):1058–1062, 2012.

[18] David Diaz Reigosa, Juan Manuel Guerrero, Alberto B. Diez, and Fernando Briz. Rotor temperature estimation in doubly-fed induction machines using rotating high-frequency signal injection. *IEEE Transactions on Industry Applications*, 53(4):3652–3662, July 2017.

[19] R. Ibtiouen, S. Mezani, O. Touhami, N. Nouali, and M. Benhaddadi. Application of lumped parameters and finite element methods to the thermal modeling of an induction motor. In *IEMDC 2001. IEEE International Electric Machines and Drives Conference (Cat. No.01EX485)*, IEMDC-01, page 505–507. IEEE.

[20] J.T. Boys and M.J. Miles. Empirical thermal model for inverter-driven cage induction machines. *IEE Proceedings - Electric Power Applications*, 141(6):360–372, November 1994.

[21] A. Arkkio. Unbalanced magnetic pull in cage induction motors with asymmetry in rotor structures. In *Eighth International Conference on Electrical Machines and Drives*, volume 1997, page 36–40. IEE, 1997.

[22] P. L. Alger. The magnetic noise of polyphase induction motors [includes discussion]. *Transactions of the American Institute of Electrical Engineers. Part III: Power Apparatus and Systems*, 73(2):118–125, April 1954.

[23] I. Hirotsuka, K. Tsuboi, and F. Ishibashi. Effect of slot-combination on electromagnetic vibration of squirrel-cage induction motor under loaded condition. In *Proceedings of Power Conversion Conference - PCC '97*, volume 2 of *PCCON-97*, page 843–848. IEEE.

[24] T. Gundogdu, Z. Q. Zhu, J. C. Mipo, and P. Farah. Influence of magnetic saturation on rotor bar current waveform and performance in induction machines. In *2016 XXII International Conference on Electrical Machines (ICEM)*, page 391–397. IEEE, September 2016.

[25] T. Gundogdu, Z. Q. Zhu, and J. C. Mipo. Influence of stator slot and pole number combination on rotor bar current waveform and performance of induction machines. In *2017 20th International Conference on Electrical Machines and Systems (ICEMS)*, page 1–6. IEEE, August 2017.

[26] T. Gundogdu, Z. Q. Zhu, J. C. Mipo, and P. Farah. Investigation of non-sinusoidal rotor bar current phenomenon in induction machines — influence of slip and electric loading. In *2016 XXII International Conference on Electrical Machines (ICEM)*, page 419–425. IEEE, September 2016.

[27] Victor Goman, Vladimir Prakht, Vladimir Dmitrievskii, and Fedor Sarapulov. Analysis of coupled thermal and electromagnetic processes in linear induction motors based on a three-dimensional thermal model. *Mathematics*, 10(1):114, December 2021.

[28] Farshid Mahmouditabar and Nick J. Baker. Design optimization of induction motors with different stator slot rotor bar combinations considering drive cycle. *Energies*, 17(1):154, December 2023.

[29] An Zhao, Giovanni Zanuso, and Luca Peretti. Transient thermal models of induction machines under inter-turn short-circuit fault conditions. *IET Electric Power Applications*, 17(10):1304–1320, June 2023.

[30] Peer-Ole Gronwald and Thorsten Alexander Kern. Experimental validation and parameter study of a 2d geometry-based, flexible designed thermal motor model for different cooled traction motor drives. *World Electric Vehicle Journal*, 12(2):76, May 2021.